

Theoretical analysis of a nanoscale plasmonic filter based on a rectangular metal–insulator–metal waveguide

This content has been downloaded from IOPscience. Please scroll down to see the full text.

2010 J. Phys. D: Appl. Phys. 43 385102

(<http://iopscience.iop.org/0022-3727/43/38/385102>)

View [the table of contents for this issue](#), or go to the [journal homepage](#) for more

Download details:

IP Address: 115.156.166.115

This content was downloaded on 25/12/2014 at 07:03

Please note that [terms and conditions apply](#).

Theoretical analysis of a nanoscale plasmonic filter based on a rectangular metal–insulator–metal waveguide

Binfeng Yun, Guohua Hu and Yiping Cui¹

Advanced Photonics Center, Southeast University, Nanjing 210096, People's Republic of China

E-mail: ybf@seu.edu.cn, photonics@seu.edu.cn and cyp@seu.edu.cn


Received 20 June 2010, in final form 22 July 2010

Published 7 September 2010

Online at stacks.iop.org/JPhysD/43/385102

Abstract

A compact and nanometric surface plasmon polariton (SPP) band-pass filter based on a rectangular ring resonator composed of metal–insulator–metal waveguides is proposed. Using the finite difference time domain method, the effects of the structure parameters on the transmission characteristics of this SPP band-pass filter are analysed in detail. The results show that the proposed SPP filter has narrow transmission peaks and the corresponding resonance wavelengths can be linearly tuned by altering the resonator's cavity length. Moreover, the transmission ratios of the pass bands can be tuned by changing the coupling gaps between the input/output MIM waveguides and the resonator. Also the metal loss and dispersion effects on the filter responses are included. The simple band-pass SPP filter is very promising for high-density SPP waveguide integrations.

 Online supplementary data available from stacks.iop.org/JPhysD/43/385102/mmedia

(Some figures in this article are in colour only in the electronic version)

1. Introduction

Surface plasmon polaritons (SPPs) are electromagnetic waves coherently coupled to electron oscillations and propagating at the interface between a dielectric and a metal, evanescently confined in the perpendicular direction [1, 2]. SPP waveguides are very promising for subwavelength scale integration, which cannot be realized by the traditional dielectric waveguides because of the diffraction limit. There are two basic types of SPP waveguides, which are based on the insulator–metal–insulator (IMI) structure [3–5] and the metal–insulator–metal (MIM) structure [6–8]. The mode sizes of the IMI SPP waveguides are on the order of micrometres and their propagation lengths can reach up to millimetres, while the mode sizes of the MIM SPP waveguides can be restricted to the nanometre scale and their propagation lengths are reduced to the micrometre scale. Because of the nanoscale mode sizes, the components based on the MIM SPP waveguides are very promising for optical signal propagation and processing in future high-density integration platforms. Until now, different

SPP waveguide components based on the MIM structure have been demonstrated, such as bends and splitters [9, 10], Mach–Zehnder interferometers [11], Y-shaped combiners [12] and wavelength sorters [13]. SPP filters are one kind of the key components in the SPP integration platform. Different SPP filter structures based on the MIM waveguides have been proposed recently, including ring resonator filters [14–17], tooth-shaped filters [18, 19] and Bragg grating filters [20–23]. Most of these SPP filters are band-stop type, but band-pass-type SPP filters are also very important and useful in nanometric SPP waveguide integrations. Recently, a nanometric band-pass filter based on a SPP circular ring resonator has been proposed [17]. Here with the merit of a very high transmission at 90° bends, which is impossible for the dielectric waveguide [9, 10], miniaturized rectangular ring resonators can be realized with the MIM SPP waveguides. Also, compared with the circular ring resonator, the SPP filter with rectangular geometry is easier to fabricate. In this paper, the transmission characteristics of band-pass SPP filters based on rectangular geometry are investigated by the finite difference time domain (FDTD) method, with the perfect matching layer absorbing boundary conditions. The results

¹ Author to whom any correspondence should be addressed.

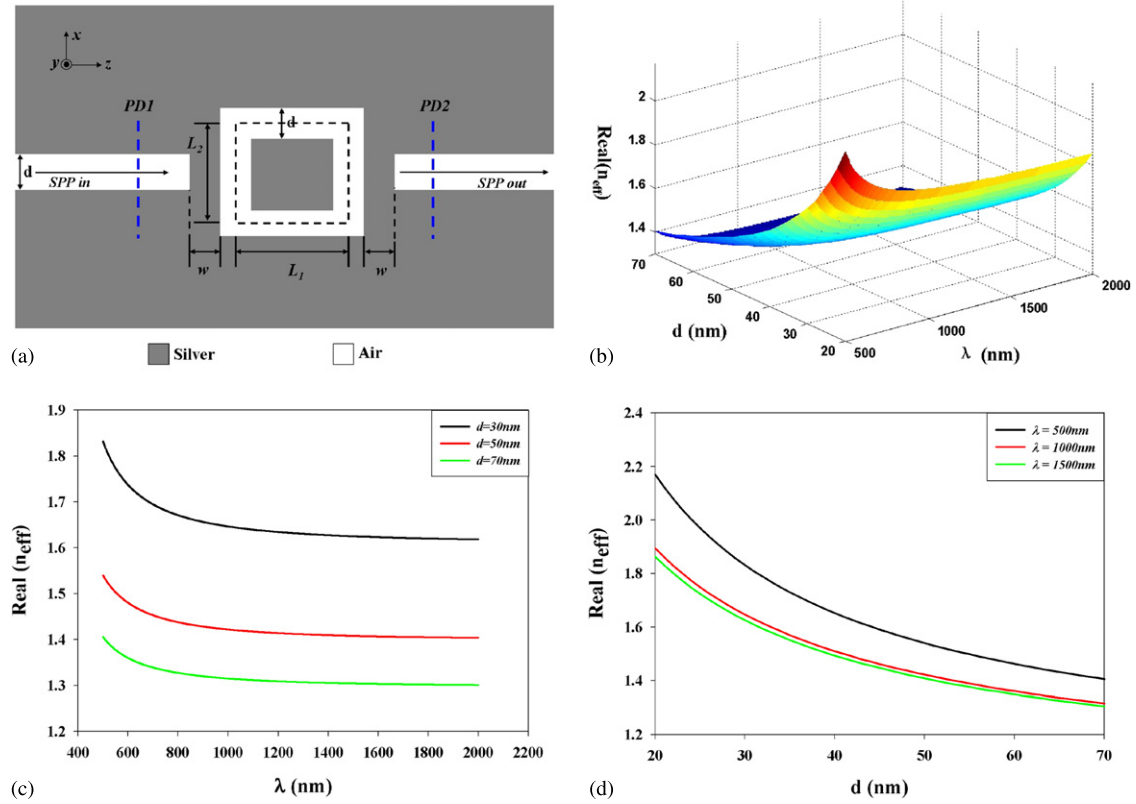


Figure 1. (a) The SPP filter structure composed of a rectangular resonance cavity based on MIM waveguides. (b)–(d) The dependence of $\text{Re}(n_{\text{eff}})$ of the fundamental TM mode on the wavelength λ of incident light and the waveguide width d .

show that with properly designed ultra-small resonance cavity structures, **multi-order transmission peaks** can be realized and both the resonance wavelengths and the transmission ratio can be tuned by adjusting the structure parameters. Also some different configurations of the MIM SPP filters are presented and analysed.

2. FDTD modelling method

2.1. The schematic of the SPP filter and its resonance transmission spectrum

Figure 1(a) shows the structure of the proposed MIM SPP filter based on rectangular geometry which is composed of an input MIM waveguide, **a rectangular MIM ring resonator** and an output MIM waveguide. The structure parameters d , w , L_1 and L_2 are the width of the MIM waveguide, the gap size between the input/output MIM waveguides and the rectangular MIM ring resonator and the side length of the rectangular MIM ring resonator, respectively. For MIM waveguides, only the **transverse magnetic (TM) modes** can be supported. And in this paper, the MIM waveguide width $d = 50$ nm is set to ensure that only the fundamental TM mode is supported, while the other modes are cut off. The dispersion relation of the fundamental TM mode in a MIM waveguide is given by [18]

$$\varepsilon_{\text{in}} k_{z2} + \varepsilon_m k_{z1} \coth\left(-\frac{ik_{z1}}{2}d\right) = 0, \quad (1)$$

and k_{z1} and k_{z2} are

$$k_{z1}^2 = \varepsilon_{\text{in}} k_0^2 - \beta^2, \quad k_{z2}^2 = \varepsilon_m k_0^2 - \beta^2, \quad (2)$$

where ε_{in} , ε_m and $k_0 = 2\pi/\lambda$ are the dielectric constants of the insulator (air) and the metal (silver), and the free-space wave vector, respectively. The dielectric constant of the metal silver is characterized by the Lorentz–Drude model [17, 24]:

$$\varepsilon_m = \varepsilon_{\infty} - \sum_{m=0}^5 \frac{G_m \Omega_m^2}{\omega_m^2 - \omega^2 + i\omega\Gamma_m}, \quad (3)$$

where ε_{∞} is the relative permittivity at infinite frequency, G_m is the oscillator strength, Ω_m is the plasma frequency, ω is the angular frequency of incident light, and all these parameters are listed in [24]. The real part of the effective index of the fundamental TM mode ($n_{\text{eff}} = \beta/k_0$) as a function of the MIM waveguide width d and the incident light wavelength λ is shown in figures 1(b)–(d). n_{eff} decreases as d increases and decreases relatively slowly as λ increases.

The 2D FDTD method with the **perfect matched layer boundary condition** is used to simulate the transmission spectra of the SPP filters. The fundamental TM mode of the MIM waveguide is excited by a pulse source and the mesh grid size is set to 1 nm in order to maintain convergence. Two power monitors PD1 and PD2 are set to detect the incident power A_1 (without the MIM rectangular ring resonator) and the transmitted power A_2 (with the MIM rectangular ring resonator), and the transmittance is defined

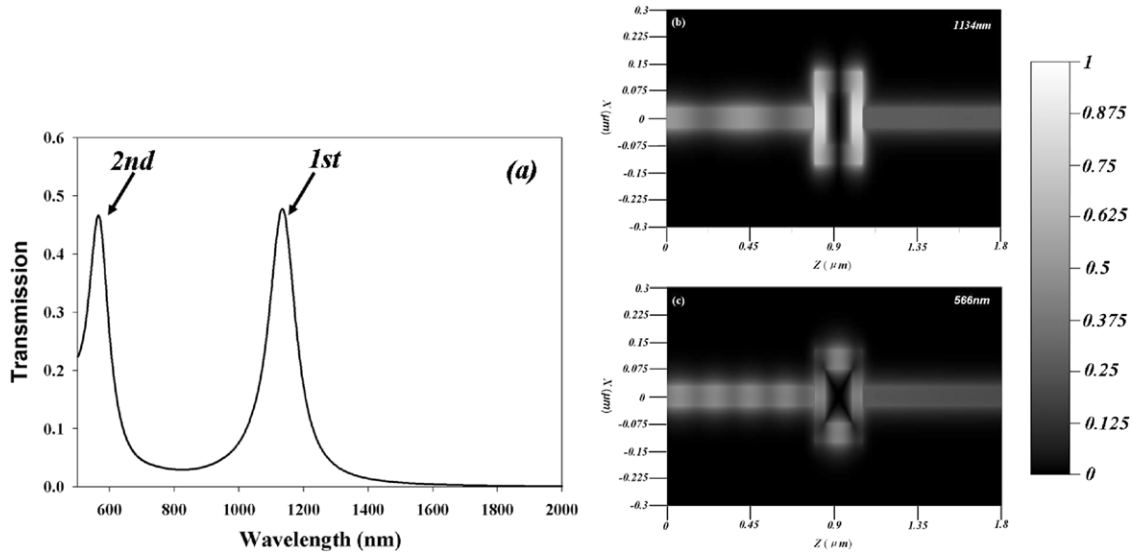


Figure 2. (a) The transmission spectrum of the SPP filter with square geometry ($L_1 = L_2 = 200$ nm). (b) The normalized $|H_y|$ field patterns of the square SPP filter at the first resonance wavelength of 1134 nm. (c) The normalized $|H_y|$ field patterns of the square SPP filter at the second resonance wavelength of 566 nm.

as $T = A_2/A_1$ [17]. The simulated transmission spectrum of the SPP filter with square geometry ($L_1 = L_2 = 200$ nm) is shown in figure 2(a). It is obvious that there are two resonance peaks in the wavelength range 500–2000 nm. The total MIM waveguide length in the rectangular ring cavity (cavity length) is the average length of the inner and outer perimeters, $L = 2(L_1 + L_2) = 800$ nm, as depicted by the dashed line in figure 1(a) [15]. The resonance condition for the rectangular ring cavity is [15, 17]

$$L = N\lambda_{\text{spp}} = N(\lambda/\text{Re}(n_{\text{eff}})), \quad (N = 1, 2, 3, \dots). \quad (4)$$

In figure 2(a), the wavelengths of the first ($N = 1$) resonance peak and the second ($N = 2$) resonance peak are 1134 nm and 566 nm, respectively. As shown in figure 1(b), the $\text{Re}(n_{\text{eff}})$ of the MIM waveguides at 1134 nm and 566 nm are 1.4163 and 1.4949, respectively. According to equation (4), the theoretical resonance length for the first resonance peak is $L_{\text{res}} = 800.7$ nm, which fits the actual cavity length $L = 800$ nm well, while $L_{\text{res}} = 757.2$ nm for the second resonance peak is shifted relative to the actual cavity length $L = 800$ nm. Also, the normalized $|H_y|$ fields at the first and the second resonance transmission peaks are shown in figures 2(b) and (c), respectively (see also supplementary animations S1 (stacks.iop.org/JPhysD/43/385102/mmedia) and S2 (stacks.iop.org/JPhysD/43/385102/mmedia)). It is obvious that the standing waves are formed by the interference of the clockwise travelling SPP wave and the anticlockwise travelling SPP wave in the resonance cavity. Moreover, according to the normalized $|H_y|$ field patterns in the square resonator cavities, the maximum transmission peaks at 1134 nm and 566 nm correspond to the resonating conditions $L = \lambda_{\text{spp}}$ and $L = 2\lambda_{\text{spp}}$, respectively.

2.2. Transmission characteristics of SPP resonator with square geometry

In order to study the effects of cavity lengths on the transmission spectra of the SPP filters, SPP filters with various

cavity lengths are simulated and the results are shown in figure 3. Figure 3(a) shows the transmission spectra of the SPP filters with total cavity lengths of 600, 720 and 800 nm. Figure 3(b) shows the relations between the wavelengths of transmission peaks (resonance wavelengths) and the resonance cavity lengths L with gap sizes of $w = 10$ nm and $w = 20$ nm. It is clear from figure 3(a) that both the first and second transmission peaks are red shifted with increasing cavity lengths. And as shown in figure 3(b), the first and second resonance wavelengths can be linearly tuned by altering the cavity lengths of the SPP filters. The reason is that if the cavity length is increased, the resonance wavelength must be increased to maintain the resonance condition of equation (4). Also as shown in figure 3(b), the resonance wavelengths of the SPP filters with gap size $w = 20$ nm are smaller than those of the SPP filters with gap size $w = 10$ nm, which are same as the circular ring resonator [17]. Moreover, the first resonance wavelength differences between the SPP filters with gap sizes $w = 10$ nm and $w = 20$ nm are larger than those of the second resonances. The reason is that the effective index (n_{eff}) of the first resonance (at a shorter wavelength) is larger than that of the second resonance according to figure 1(c). In the coupling region, the effective index variation can be caused by the coupling effect, and the effective index variation of the second resonance has a lesser effect on n_{eff} than that of the first resonance. Hence the first resonance wavelength differences between the SPP filters with gap sizes $w = 10$ nm and $w = 20$ nm are larger than those of the second resonances according to the resonance condition (equation (4)).

The transmission spectra of the SPP filters with different gap sizes w are simulated and the results are shown in figure 4(a). It is obvious that the peak transmission values of the SPP filters decrease with increasing gap size w . This is because the coupling strength between the input/output MIM waveguide and the rectangular SPP resonator is related to

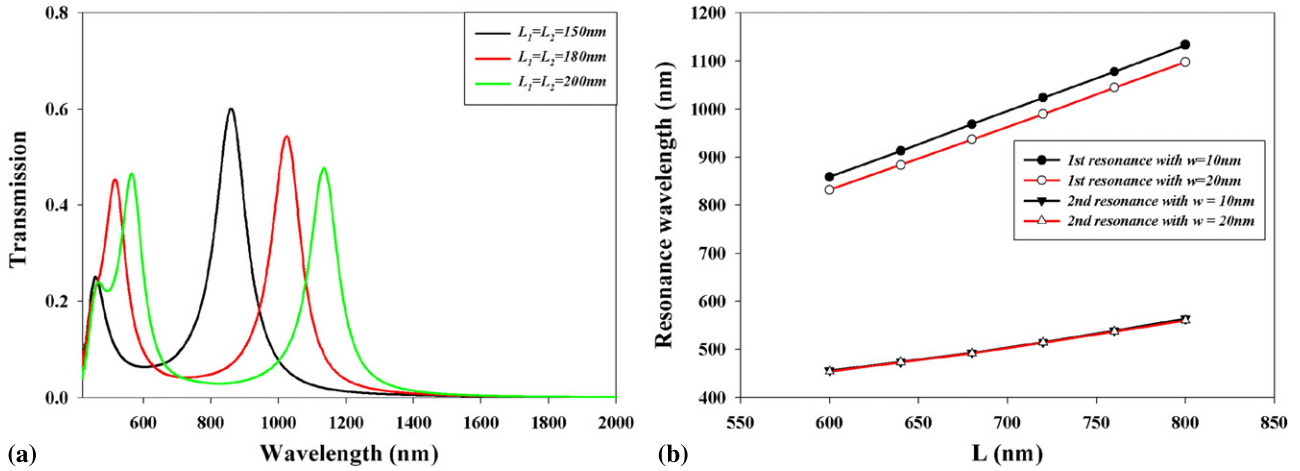


Figure 3. (a) The transmission spectra of the SPP filter with different cavity lengths ($w = 10\text{ nm}$, $d = 50\text{ nm}$). (b) The wavelengths of the transmission peaks as a function of the cavity lengths with gap size $w = 10\text{ nm}$ and $w = 20\text{ nm}$, respectively.

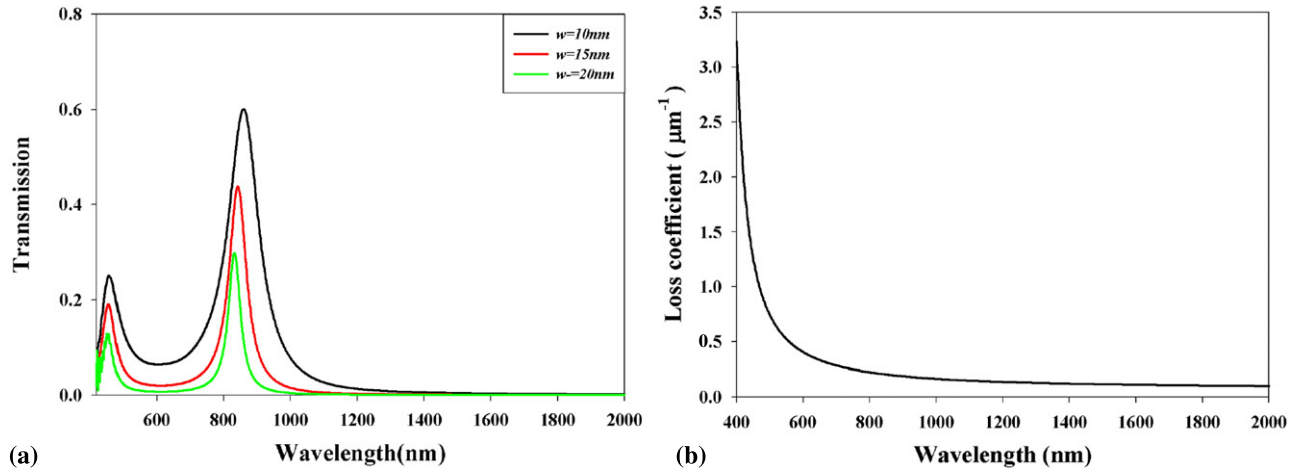


Figure 4. (a) The transmission spectra of the SPP filter with different gap sizes ($L_1 = L_2 = 150\text{ nm}$, $d = 50\text{ nm}$). (b) The imaginary part of the effective index of the MIM waveguide ($d = 50\text{ nm}$) as a function of wavelength.

the gap size. The smaller the gap size w , the larger the coupling strength and much more SPP power can be coupled into and coupled out of the resonance cavity. Also, as shown in figure 4(a), a very small resonance wavelength shift exists for the filters with different gap sizes w . This is because the effective refractive index in the coupling region is different from that of the standard MIM waveguide [17], and the smaller the gap size w , the more is the deviation. Also the differences between the resonance wavelengths of the SPP filters with $w = 10\text{ nm}$ and those with $w = 20\text{ nm}$ in figure 3(b) are caused by this fact.

In figure 3(a), in addition to the resonance wavelength shifts for various resonator cavity lengths, another phenomenon can also be clearly observed. The transmission peak of the first resonance decreases with increasing cavity length, while that of the second resonance increases with increasing cavity length. At first glance, the transmission peaks of the resonances should decrease with increasing cavity lengths because the longer the cavity lengths, the longer the paths that the SPP waves pass through and more absorption should be caused by the metal. However, a dispersive loss coefficient

should also be considered for the MIM SPP waveguide because the total cavity loss is affected by the combinational effects of the cavity length and the loss coefficient. The loss coefficient ($\alpha = 4 \times \pi \times \text{Im}(n_{\text{eff}})/\lambda$) of the MIM waveguide is calculated as shown in figure 4(b). From figure 4(b), it is clear that the loss coefficient decreases with increasing wavelength. Moreover, the loss coefficient decays very fast in the wavelength range 400–600 nm, while it decays very slowly when the wavelength is longer than 600 nm. The transmission peaks of the first resonances decrease with increasing wavelength in figure 3(a) because the total cavity losses are dominated by increasing cavity lengths when the loss coefficients decrease slowly, while the transmission peaks of the second resonances which increase with increasing wavelength are caused by the very fast decay of the loss coefficients which dominate the total cavity loss.

During the fabrication, it is inevitable that there may be location shifts Δh between the input MIM waveguide and the output MIM waveguide as shown in figure 5(a). In order to study the effects of the location shift Δh on the transmission characteristics, the transmission spectra of the

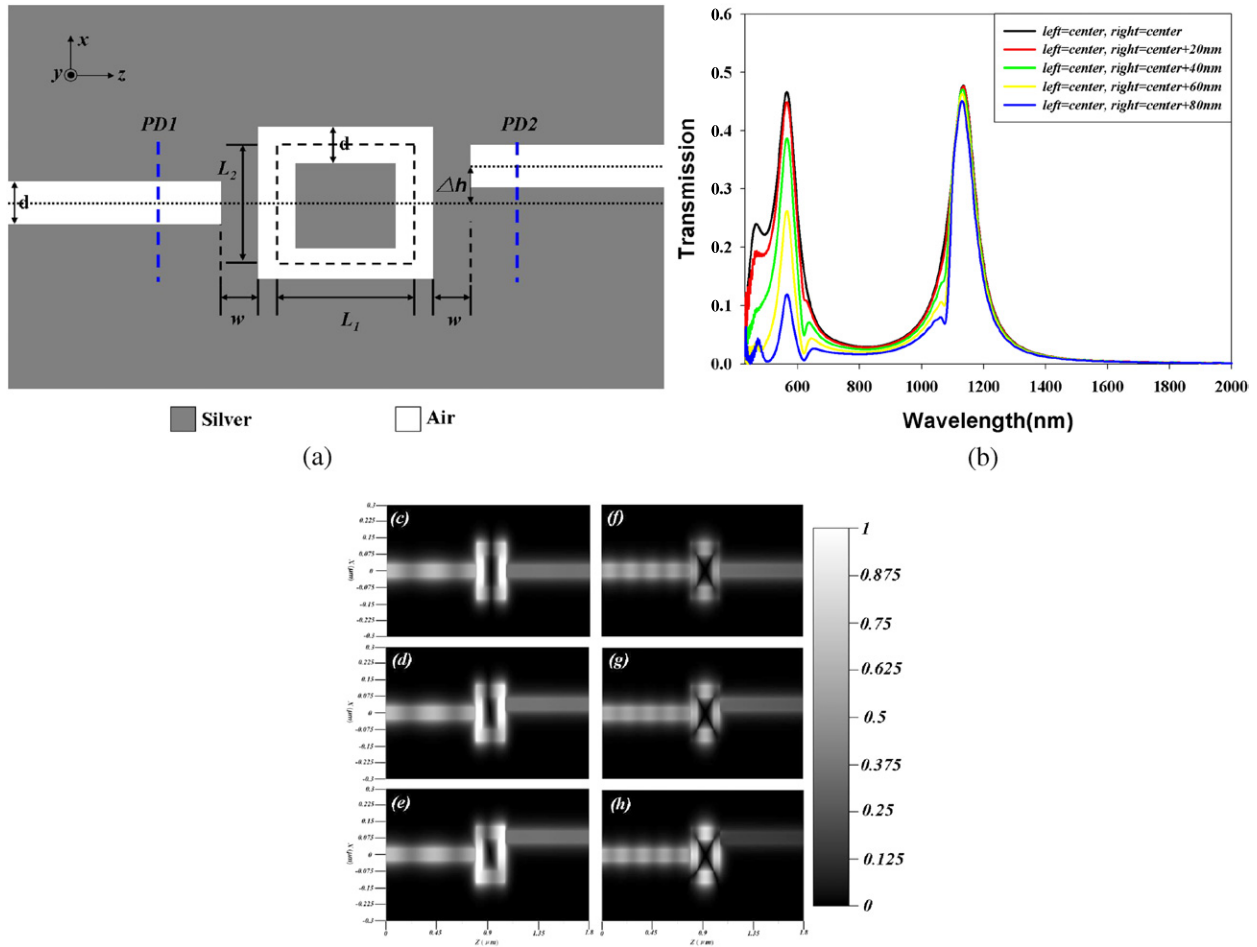


Figure 5. (a) The schematic of the square SPP filter with different output MIM waveguide shifts Δh . (b) The transmission spectra of the square SPP filter with different output MIM waveguide shifts Δh ($L_1 = L_2 = 200$ nm, $w = 10$ nm). (c)–(e) The normalized $|H_y|$ field patterns of the square SPP filter at the first resonance wavelengths with $\Delta h = 0$ nm, 40 nm and 80 nm, respectively. (f)–(h) The normalized $|H_y|$ field patterns of the square SPP filter at the second resonance wavelengths with $\Delta h = 0$ nm, 40 nm and 80 nm, respectively.

SPP filters with different Δh are simulated and the results are shown in figure 5(b). Both the first and second resonance wavelengths are almost not affected by the location shift Δh because the cavity lengths are kept constant. And it is interesting that with increasing location shift Δh , the first resonance transmission peak values are almost the same, but the second resonance transmission peak values are quickly reduced. In order to explain this phenomenon, the normalized $|H_y|$ field patterns of the SPP filters at the first and second resonance wavelengths are shown in figures 5(c)–(h). For the first resonance, when the location shift alters from $\Delta h = 0$ to $\Delta h \neq 0$, the standing wave in the resonance cavity changes to a travelling wave (see also supplementary animation S3 (stacks.iop.org/JPhysD/43/385102/mmedia)). And it is obvious that the locations of the maximum $|H_y|$ fields of the travelling waves are shifted according to the shifted output MIM waveguides. For the second resonance, only standing waves can be realized in the resonance cavity even when $\Delta h \neq 0$ (see also supplementary animation S4 (stacks.iop.org/JPhysD/43/385102/mmedia)). Hence the locations of the maximum $|H_y|$ fields are kept at the centres of the four sides of the square resonance cavity. With the normalized $|H_y|$ field distributions shown

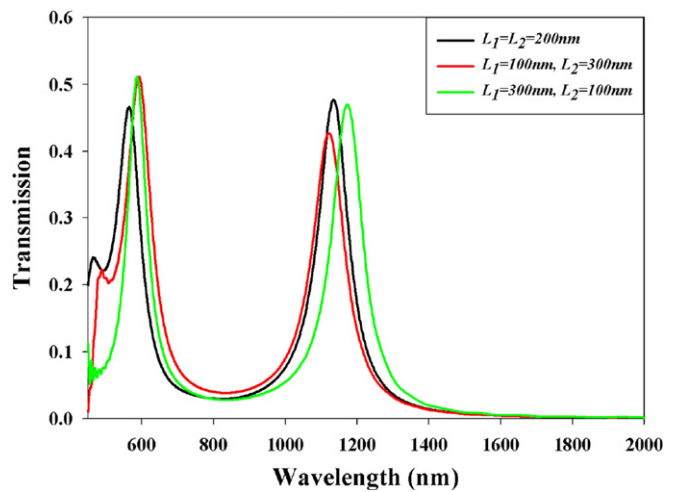


Figure 6. The transmission spectra of the SPP filter with square resonance cavity and the rectangular resonance cavities (with the same total cavity length of $L = 800$ nm, $w = 10$ nm).

in figures 5(c)–(h), the characteristics of the first and second resonance transmission peak values can be explained.

Also in order to investigate the effects of the geometries of the resonance cavities, the transmission spectra of the

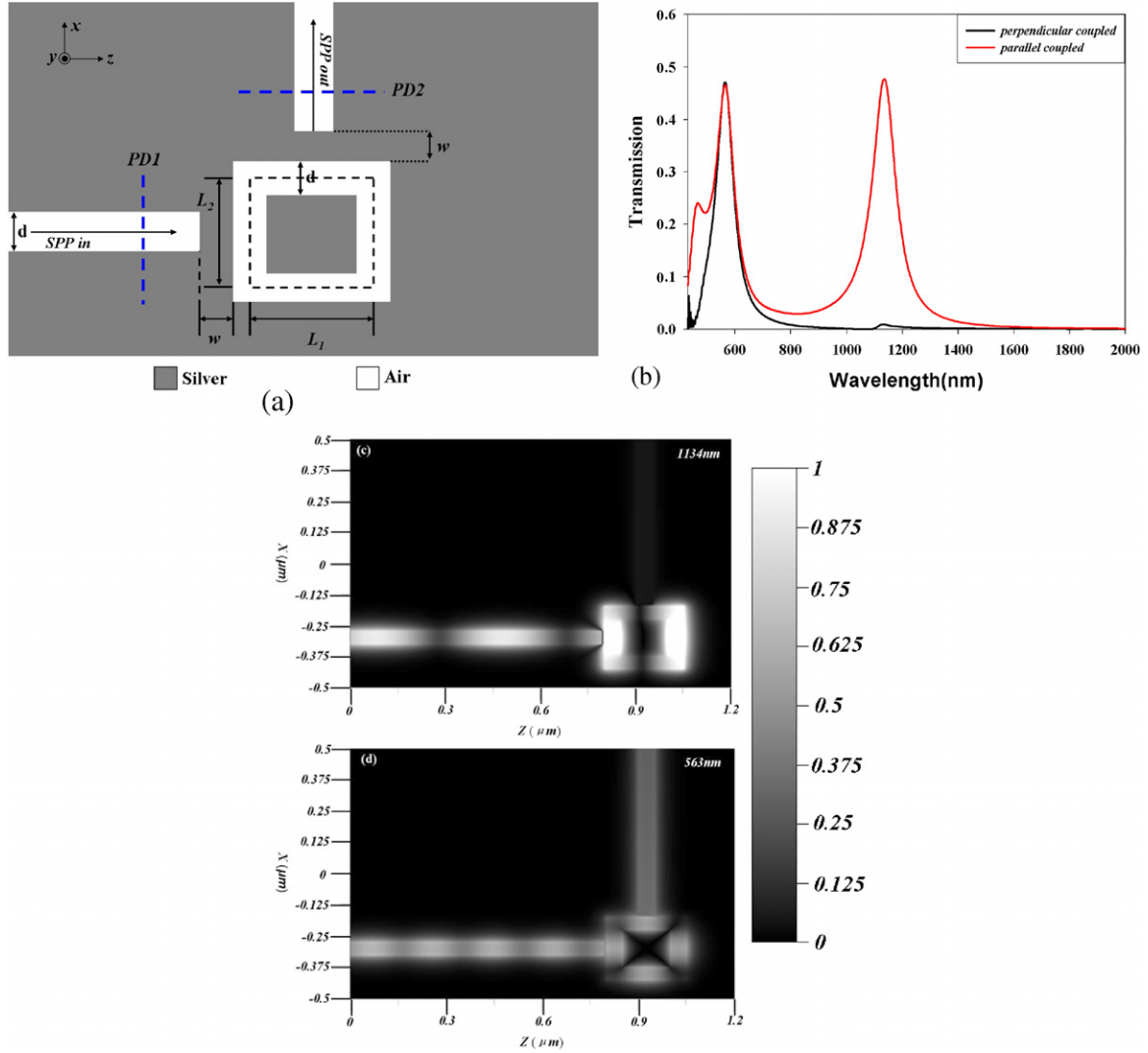


Figure 7. (a) The schematic of the SPP filter with perpendicular output ($L_1 = L_2 = 200$ nm). (b) Comparison of the transmission spectra for the SPP filter with perpendicular output and parallel output. (c) The normalized $|H_y|$ field patterns of the square SPP filter at the first resonance wavelength of 1134 nm. (d) The normalized $|H_y|$ field patterns of the square SPP filter at the second resonance wavelength of 563 nm.

SPP filters with **square** resonance cavities and **rectangular** resonance cavities, which have the same total cavity length of $L = 800$ nm, are simulated and the results are shown in figure 6. The results show that the first and second resonance peaks can be both affected by the geometries of the resonance cavities.

2.3. Different configurations of the proposed SPP filter

There are some **different input/output configurations** of the proposed SPP filters. One of them is the SPP filter with **perpendicular output**, as shown in figure 7(a). Figure 7(b) shows the transmission spectrum of this configuration, and the transmission spectrum of the SPP filter with a parallel output configuration is also plotted for comparison. **Compared with the parallel output configuration, the first resonance peak of the perpendicular output is significantly reduced near to zero while the second resonance peak remains unchanged.** This can be illustrated by the normalized $|H_y|$ field distributions in

the resonance cavities, as shown in figures 7(c) and (d). **This is because when the SPP wave couples into the rectangular resonance cavity, the standing waves, as shown in figures 7(c) and (d), are formed by the interference of the clockwise travelling SPP wave and the anticlockwise travelling SPP wave.** According to the phase-matching condition, for the first resonance, two **antinodes** are formed at the two vertical sides of the rectangular cavity and the nodes are formed at the two parallel sides. Hence no SPP wave can be coupled from the parallel sides to the perpendicular output MIM waveguide. While for the second resonance, four antinodes are formed at the four sides of the rectangular cavity, so the SPP wave power can be coupled into the perpendicular output.

Finally, a SPP filter with two perpendicular outputs, as shown in figure 8(a), is investigated and the transmission spectra at the two outputs are plotted in figure 8(b). Also the normalized $|H_y|$ field distributions at the first and second resonance wavelengths are shown in figures 8(c) and (d). It is clear that at the first resonance peak, the input SPP power

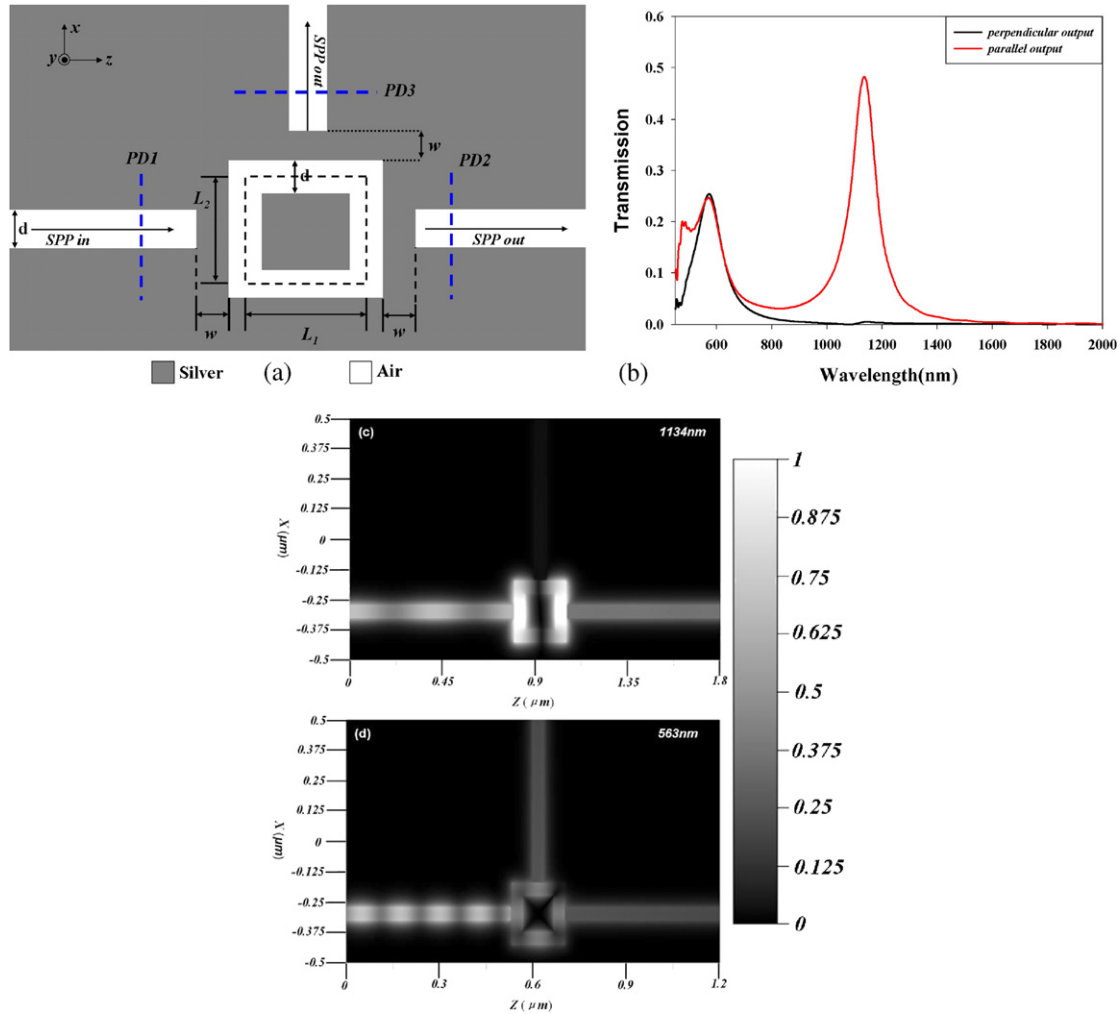


Figure 8. (a) The schematic of the SPP filter with two perpendicular outputs ($L_1 = L_2 = 200$ nm). (b) The transmission spectra for the SPP filter with two perpendicular outputs. (c) The normalized $|H_y|$ field patterns of the square SPP filter at the first resonance wavelength of 1134 nm. (d) The normalized $|H_y|$ field patterns of the square SPP filter at the second resonance wavelength of 563 nm.

is well coupled to the parallel output, while almost no SPP power is coupled to the perpendicular output. At the second resonance peak, the SPP power is equally coupled to the two outputs. The reason is the same as shown in figures 7(c) and (d). For the first resonance, two antinodes are formed at the two vertical sides of the rectangular cavity and the nodes are formed at the two parallel sides. Hence no SPP wave can be coupled from the parallel sides to the perpendicular output MIM waveguide (see also supplementary animation S5 (stacks.iop.org/JPhysD/43/385102/mmedia)). While for the second resonance, four antinodes are formed at the four sides of the rectangular cavity, hence the SPP wave power can be equally coupled into the parallel output and the perpendicular output (see also supplementary animation S6 (stacks.iop.org/JPhysD/43/385102/mmedia)).

3. Conclusions

In this paper, a nanometric SPP band-pass filter based on a rectangular resonator is proposed and analysed numerically. The influences of the structure parameters on the transmission characteristics of the SPP filter are analysed in detail. The

results show that multiple resonance transmission peaks could be realized and the resonance wavelengths can be easily tuned by altering the cavity lengths. The peak transmission ratios of the SPP filters are decreased with increasing gap size w , while the resonating wavelengths are almost unchanged. Also, the resonance transmission ratios are determined by the combinational effects of the cavity lengths and the loss coefficient of the dispersive MIM waveguide. By the shifting of the output waveguides, the resonance wavelengths of the first and second transmission peaks are almost not affected, but the effects on transmission ratios of the two resonance peaks are obviously different. Finally, two different configurations of the proposed SPP filter are demonstrated and analysed. In conclusion, the proposed SPP band-pass filters with various configurations are very promising for high-density SPP waveguide integrations.

Acknowledgments

This work was supported by the National Science Foundation of China under Grant No 60907025 and the Science Foundation of Southeast University under Grant No KJ2009358.

References

- [1] Barnes W L, Dereux A and Ebbesen T W 2003 *Nature* **124** 824
- [2] Ozbay E 2006 *Science* **311** 189
- [3] Berini P 2009 *Adv. Opt. Photon.* **1** 484
- [4] Kim J T, Ju J J, Park S, Kim M-S, Park S K and Lee M-H 2008 *Opt. Express* **16** 13133
- [5] Yun B, Hu G and Cui Y 2009 *Opt. Express* **17** 3610
- [6] Bozhevolnyi S I, Volkov V S, Devaux E, Laluet J-Y and Ebbesen T W 2006 *Nature* **440** 508
- [7] Bozhevolnyi S I, Volkov V S, Devaux E and Ebbesen T W 2005 *Phys. Rev. Lett.* **95** 046802
- [8] Yun B, Hu G, Ji Y and Cui Y 2009 *J. Opt. Soc. Am. B* **26** 1924
- [9] Veronis G and Fan S 2005 *Appl. Phys. Lett.* **87** 131102
- [10] Lee T-W and Gray S K 2005 *Opt. Express* **13** 9652
- [11] Han Z, Liu L and Forsberg E 2006 *Opt. Commun.* **259** 690
- [12] Gao H, Shi H, Wang C, Du C, Luo X, Deng Q, Lv Y, Lin X and Yao H 2005 *Opt. Express* **13** 10795
- [13] Kang Z and Wang G P 2008 *Opt. Express* **16** 7680
- [14] Xiao S, Liu L and Qiu M 2006 *Opt. Express* **14** 2932
- [15] Hosseini A and Massoud Y 2007 *Appl. Phys. Lett.* **90** 181102
- [16] Han Z, Van V, Herman W N and Ho P T 2009 *Opt. Express* **17** 12678
- [17] Wang T-B, Wen X-W, Yin C-P and Wang H-Z 2009 *Opt. Express* **17** 24096
- [18] Lin X-S and Huang X-G 2008 *Opt. Lett.* **33** 2874
- [19] Tao J, Huang X, Lin X, Chen J, Zhang Q and Jin X 2010 *J. Opt. Soc. Am. B* **27** 323
- [20] Wang B and Wang G P 2005 *Appl. Phys. Lett.* **87** 013107
- [21] Hosseini A and Massoud Y 2006 *Opt. Express* **14** 11318
- [22] Liu J-Q, Wang L-L, He M-D, Huang W-Q, Wang D, Zou B S and Wen S 2008 *Opt. Express* **16** 4888
- [23] Gong Y, Wang L, Hu X, Li X and Liu X 2009 *Opt. Express* **17** 13727
- [24] Rakic A D, Djuricic A B, Elazar J M and Majewski M L 1998 *Appl. Opt.* **37** 5271